

The splicing regulator Rbfox1 (A2BP1) controls neuronal excitation in the mammalian brain

Lauren T Gehman¹, Peter Stoilov², Jamie Maguire³, Andrey Damianov⁴, Chia-Ho Lin⁴, Lily Shiue⁵, Manuel Ares Jr⁵, Istvan Mody^{6,7} & Douglas L Black^{1,4,8}

The Rbfox family of RNA binding proteins regulates alternative splicing of many important neuronal transcripts, but its role in neuronal physiology is not clear¹. We show here that central nervous system-specific deletion of the gene encoding Rbfox1 results in heightened susceptibility to spontaneous and kainic acid-induced seizures. Electrophysiological recording revealed a corresponding increase in neuronal excitability in the dentate gyrus of the knockout mice. Whole-transcriptome analyses identified multiple splicing changes in the *Rbfox1*^{-/-} brain with few changes in overall transcript abundance. These splicing changes alter proteins that mediate synaptic transmission and membrane excitation. Thus, Rbfox1 directs a genetic program required in the prevention of neuronal hyperexcitation and seizures. The Rbfox1 knockout mice provide a new model to study the post-transcriptional regulation of synaptic function.

Alternative pre-mRNA splicing is an important mechanism for regulating gene expression in the central nervous system (CNS), where it both affects neuronal development and controls functions in the mature brain^{2,3}. Developmental and tissue-specific alternative splicing is mediated by *cis*-acting elements in the pre-mRNA and by corresponding *trans*-acting protein factors that bind these elements to influence adjacent spliceosome assembly. The RNA-binding Fox (Rbfox) family of splicing factors is comprised of three members, Rbfox1 (Fox-1 or A2BP1), Rbfox2 (Fox-2 or RBM9) and Rbfox3 (Fox-3, HRNBP3 or NeuN). Rbfox proteins regulate splicing of many neuronal transcripts by binding the sequence (U)GCAUG in introns flanking alternative exons⁴⁻⁷. A (U)GCAUG motif that lies downstream of the alternative exon generally promotes Rbfox-dependent exon inclusion, whereas an upstream motif will usually repress exon inclusion^{4,6,8-12}. Human RBFOX1 (A2BP1) was first identified through its interaction with Ataxin-2, the protein mutated in spinocerebellar ataxia type II¹³. Critical neurological functions for Rbfox1 are indicated by human mutations in *RBFOX1* that lead to severe disorders including mental retardation, epilepsy and autism spectrum disorder¹⁴⁻¹⁷.

The three mouse Rbfox paralogues show a high degree of sequence conservation, especially within the RNA binding domain, which is identical in Rbfox1 and Rbfox2 and is only slightly altered in Rbfox3 (94% amino acid identity). Rbfox1 is specifically expressed in neurons, heart and muscle^{6,18}, whereas Rbfox2 is expressed in these tissues and in other cell types, including the embryo, hematopoietic cells and embryonic stem cells^{6,19,20}. Expression of Rbfox3 is limited to neurons^{21,22}. In the mature brain, most neurons express all three Rbfox paralogues, but certain neuronal subtypes and sporadic individual cells can be seen that express only one or two of the proteins²³ (Fig. 1a). All three proteins have similar N- and C-terminal domains that are diversified by alternative promoter use and alternative splicing to produce a cohort of related protein isoforms with variable localization and splicing activities^{5,24,25}. The three proteins apparently share some target exons, including exon N30 of non-muscle myosin heavy chain II-B (NMHC-B), exon N1 of *c-src* and exons 9* and 33 of the L-type calcium channel Ca_v1.2 (refs. 5,6,26).

We recently showed that the Rbfox1 transcript itself is alternatively spliced in response to chronic depolarization of cells, resulting in the increased expression of the nuclear, splicing-active Rbfox1 isoform²⁴. The change in nuclear concentration of Rbfox1 then alters the splicing of exons in multiple transcripts affecting neuronal excitation and calcium homeostasis, including the N-methyl D-aspartate (NMDA) receptor 1 (encoded by *Grin1*) and a calcium ATPase (encoded by *Atp2b1*). Thus, chronic stimulation controls the subcellular localization of Rbfox1, leading to an adaptive splicing response²⁴. Together, these findings point to a unique role for Rbfox1 in regulating neuronal gene expression. However, the effect of these Rbfox1-dependent changes on neuronal physiology in the brain is not clear. To examine the effects of Rbfox-dependent splicing within functioning neuronal circuits, we generated mice with CNS-specific deletion of Rbfox1.

We created mice carrying conditional *Rbfox1* alleles (*Rbfox1*^{loxP/loxP}; **Supplementary Fig. 1**) using standard methods and crossed them with mice carrying the Cre recombinase gene driven by the rat *Nestin* promoter and enhancer (*Nestin-Cre*^{+/-}), which express Cre in all

¹Molecular Biology Institute, University of California, Los Angeles, Los Angeles, California, USA. ²Department of Biochemistry, School of Medicine, West Virginia University, Morgantown, West Virginia, USA. ³Department of Neuroscience, Tufts University School of Medicine, Boston, Massachusetts, USA. ⁴Department of Microbiology, Immunology and Molecular Genetics, University of California, Los Angeles, Los Angeles, California, USA. ⁵Department of Molecular, Cell and Developmental Biology, Sinsheimer Labs, University of California, Santa Cruz, Santa Cruz, California, USA. ⁶Department of Neurology, The David Geffen School of Medicine, University of California, Los Angeles, Los Angeles, California, USA. ⁷Department of Physiology, The David Geffen School of Medicine, University of California, Los Angeles, Los Angeles, California, USA. ⁸Howard Hughes Medical Institute, University of California, Los Angeles, Los Angeles, California, USA. Correspondence should be addressed to D.L.B. (dough@microbio.ucla.edu).

Received 22 March; accepted 2 May; published online 29 May 2011; doi:10.1038/ng.841

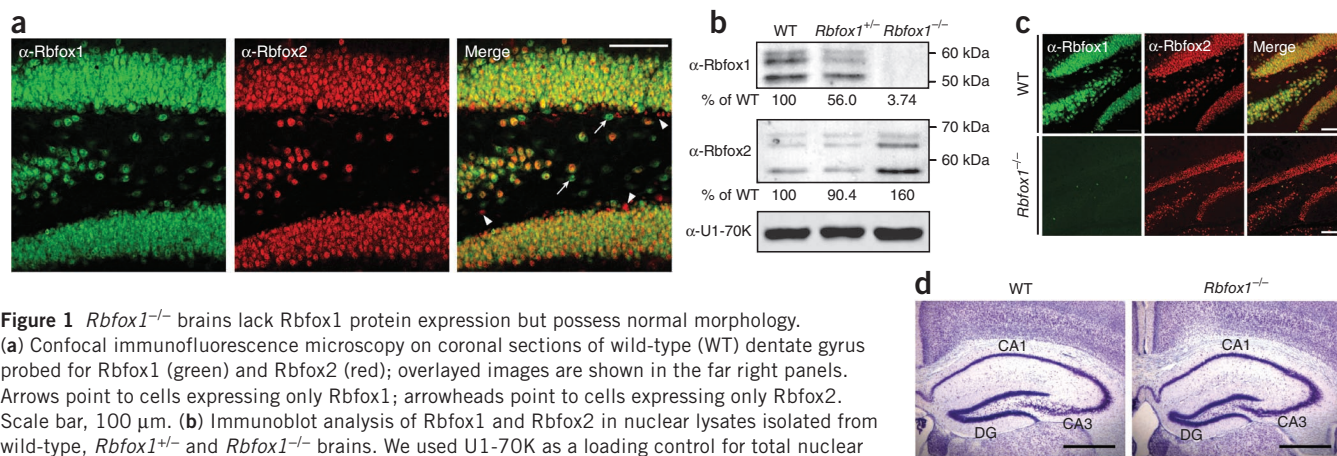


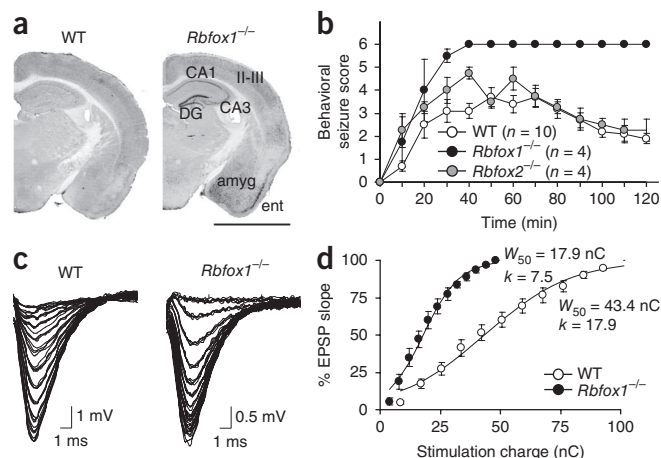
Figure 1 *Rbfox1*^{-/-} brains lack Rbfox1 protein expression but possess normal morphology. (a) Confocal immunofluorescence microscopy on coronal sections of wild-type (WT) dentate gyrus probed for Rbfox1 (green) and Rbfox2 (red); overlaid images are shown in the far right panels. Arrows point to cells expressing only Rbfox1; arrowheads point to cells expressing only Rbfox2. Scale bar, 100 μ m. (b) Immunoblot analysis of Rbfox1 and Rbfox2 in nuclear lysates isolated from wild-type, *Rbfox1*^{+/-} and *Rbfox1*^{-/-} brains. We used U1-70K as a loading control for total nuclear protein. Below each gel is the amount of Rbfox1 or Rbfox2 protein in each sample as a percentage of wild type, normalized by U1-70K expression. (c) Confocal immunofluorescence microscopy on coronal sections of wild-type and *Rbfox1*^{-/-} dentate gyrus probed for Rbfox1 (green) and Rbfox2 (red) expression. Overlaid images are shown in the far right panels. Scale bar, 100 μ m. (d) Representative Nissl stain of wild-type and *Rbfox1*^{-/-} hippocampus at 1 month of age showing normal gross morphology. Scale bar, 0.5 mm. CA1/CA3, pyramidal layers of the hippocampus; DG, dentate gyrus.

CNS stem and neural progenitor cells^{27,28}. We crossed the resulting heterozygous *Rbfox1*^{loxP/+}; *Nestin-Cre*^{+/-} mice to *Rbfox1*^{loxP/loxP} mice to obtain homozygous *Rbfox1*^{loxP/loxP}; *Nestin-Cre*^{+/-} animals. Immunoblot analysis confirmed that *Rbfox1*^{-/-} brains show loss of Rbfox1 protein (Fig. 1b). Notably, we observed a 60% increase in Rbfox2 protein expression in the *Rbfox1*^{-/-} brain, but we saw no change in Rbfox3 expression (Fig. 1b and data not shown), suggesting a cross regulation of Rbfox2 by Rbfox1 that balances overall Rbfox protein levels. By immunofluorescence, we confirmed that Rbfox1 expression is eliminated in the *Rbfox1*^{-/-} dentate gyrus and verified that localization of the homologous splicing factors Rbfox2 and Rbfox3 are unchanged in these cells (Fig. 1c and data not shown). *Rbfox1*^{loxP/loxP}; *Nestin-Cre*^{+/-} mice are viable but are slightly smaller and have reduced fertility compared to *Rbfox1*^{+/-} or wild-type littermates (data not shown). Histological analysis by Nissl staining at various postnatal stages revealed that *Rbfox1*^{-/-} brain gross morphology is normal, with no obvious anomalies in cellular architecture (Fig. 1d).

In observing the mutant mice, we found that they are prone to infrequent, spontaneous seizures under standard housing conditions. These seizures are accompanied by induction of the immediate early gene *c-fos*, an indirect marker for neuronal activity²⁹. One hour

after spontaneous seizure, *c-Fos* protein is highly expressed in the *Rbfox1*^{-/-} amygdala and hippocampus (Fig. 2a), the primary areas affected in mesial temporal lobe epilepsy³⁰. To determine if these mice also show increased susceptibility to induced seizures, we challenged them with systemic administration of kainic acid, a well described method for modeling mesial temporal lobe epilepsy³¹. We continuously evaluated the behavioral response of wild-type mice, homozygous *Rbfox1*^{loxP/loxP}; *Nestin-Cre*^{+/-} mice and heterozygous *Rbfox1*^{loxP/+}; *Nestin-Cre*^{+/-} mice by the Racine Scale³² over a two hour period after kainic acid administration (20 mg/kg, intraperitoneally; Fig. 2b and data not shown). During this period, eight out of ten wild-type mice showed relatively short tonic-clonic seizures (12.4 \pm 2.8 s). None of these mice reached stage six, defined as status epilepticus, and all survived the treatment (Fig. 2b and Supplementary Table 1). In contrast, *Rbfox1*^{loxP/loxP}; *Nestin-Cre*^{+/-} mice showed a dramatic response to kainic acid, with four out of four mice reaching status epilepticus culminating in death in under 40 min. The mean tonic-clonic seizure duration was also significantly higher in these mice than in wild-type littermates (73.2 \pm 16.8 s; $P = 0.032$). Notably, heterozygous *Rbfox1*^{loxP/+}; *Nestin-Cre*^{+/-} mice showed a kainic acid sensitivity almost identical to that of homozygous mice, with four out of four mice dying in under 40 min (Supplementary Table 1).

Figure 2 *Rbfox1*^{-/-} brains are epileptic and hyperexcitable. (a) *c-Fos* immunostaining on wild-type and *Rbfox1*^{-/-} coronal sections 1 h after a spontaneous seizure in the *Rbfox1*^{loxP/loxP}; *Nestin-Cre*^{+/-} mouse. Relevant brain areas are indicated. Amyg, amygdala; CA1/CA3, pyramidal cell layers of the hippocampus; DG, dentate gyrus; ent, entorhinal cortex; II-III indicate layers of the cerebral cortex. Scale bar, 2 mm. (b) Progression of behavioral changes after systemic kainic acid administration (20 mg/kg, intraperitoneally) in wild-type, *Rbfox1*^{loxP/loxP}; *Nestin-Cre*^{+/-} and *Rbfox2*^{loxP/loxP}; *Nestin-Cre*^{+/-} mice over a 2 h observation period. We scored seizures on the Racine Scale as described³¹, and data shown are the mean scores. Error bars, s.e.m. (c) Representative fEPSP traces from individual electrophysiological recordings in wild-type and *Rbfox1*^{-/-} dentate gyrus. (d) Average synaptic input/output (I/O) curves in wild-type and *Rbfox1*^{-/-} dentate fit with a Boltzmann function (solid lines). Circles are grand-averaged scores; error bars, s.e.m. W_{50} , stimulus width that elicits 50% of the maximum response; k , slope factor. $n = 3$ mice, 16–20 slices per experimental group.



A heterozygous deletion of *RBFOX1* was found in a human subject with epilepsy¹⁴; thus, increased susceptibility to seizure is caused by deletion of just one of the two copies of *Rbfox1* in mice and apparently humans. Notably, *Rbfox2^{loxP/loxP}; Nestin-Cre^{+/-}* mice did not show susceptibility to spontaneous or kainic acid-induced seizures (Fig. 2b and Supplementary Table 1), indicating that *Rbfox1* and *Rbfox2* are not fully redundant in their neuronal functions. The different phenotypes of the *Rbfox1* and *Rbfox2* knockout mice likely result, at least in part, from differences in their target exon sets.

To explore the physiological basis of these seizure data, we investigated changes in neuronal excitability by analyzing the synaptic input/output (I/O) relationship in wild-type and *Rbfox1^{-/-}* dentate gyrus. We measured field excitatory postsynaptic potentials (fEPSPs) in the molecular layer in response to stimulation of the lateral perforant path using varying stimulus widths. We found that the stimulus intensities required to evoke fEPSPs in the *Rbfox1^{-/-}* brain were lower than those required in wild-type brain, as shown by representative fEPSP raw traces (Fig. 2c) and average I/O curves (Fig. 2d). The grand average I/O relationships for individual experiments were fit with a Boltzmann function, where W_{50} is the stimulus width that elicits the half-maximal response and k is the slope factor. Consistent with an increase in network excitability, *Rbfox1^{-/-}* slices showed a shift to the left in the I/O relationship and a decrease in the W_{50} value to 41% that of wild-type slices (Fig. 2d). Thus, the loss of *Rbfox1* causes an increase in excitability of the neuronal population of the dentate gyrus.

To determine if the increase in excitability resulted from an increase in synapse number, we quantified spine density along granule cell dendrites of the dentate gyrus using the Golgi-Cox staining method. We found a very modest decrease in spine density along *Rbfox1^{-/-}* dendrites compared to wild-type dendrites (Supplementary Fig. 2a–c). Similarly, the *Rbfox1^{-/-}* hippocampus showed no changes in expression of the synaptic marker proteins Synapsin-I and PSD-95 (Supplementary Fig. 2d,e). Thus, altered synaptic function, rather than synapse number, is likely responsible for the increased neuronal excitability of the *Rbfox1^{-/-}* brain.

To survey the changes in exon inclusion in the *Rbfox1^{-/-}* brain compared to wild type, we used Affymetrix exon-junction (MJAY) microarrays to assay transcript abundance and alternative splicing across the genome (Supplementary Table 2). The MJAY arrays offer broad coverage but do not have probes for all exons, so to extend the analysis, we also directly assayed by RT-PCR candidate exons that are known to be regulated by *Rbfox1* or to be present in genes implicated in epilepsy. Combining the RT-PCR validated array exons and directly tested candidate exons, we identified a total of 20 statistically significant splicing changes in the *Rbfox1^{-/-}* brain compared to wild type (Table 1 and Supplementary Fig. 3). This list is not comprehensive, but compared to mice lacking other splicing factors such as *Nova³³* or *nPTB* (Qin Li & D.L.B., unpublished data), *Rbfox1* knockout mice show relatively few splicing changes in the brain. This may result from compensation for the loss of *Rbfox1* by *Rbfox2*, which is upregulated in the *Rbfox1^{-/-}* brain (Fig. 1b). The heterozygous *Rbfox1^{+/-}* brain has many of the splicing changes observed in the *Rbfox1^{-/-}* brain, but these changes are generally smaller in magnitude and show large variation between biological replicates (data not shown). Many exons altered in the *Rbfox1^{-/-}* brain also change in the *Rbfox2^{-/-}* brain, as expected from the overlap in their targets. However, some exons, including exons of the NMDA receptor 1 (encoded by *Grin1*), the voltage-gated potassium channel $K_v4.3$ (encoded by *Kcnd3*) and the L-type calcium channel $Ca_v1.3\alpha1$ (encoded by *Cacna1d*), are more responsive to loss of *Rbfox1* than *Rbfox2* (Fig. 3a). Because *Rbfox2^{loxP/loxP}; Nestin-Cre^{+/-}* mice are not prone to seizures, transcripts more strongly controlled by *Rbfox1* may have a crucial effect on the hyperexcitation phenotype.

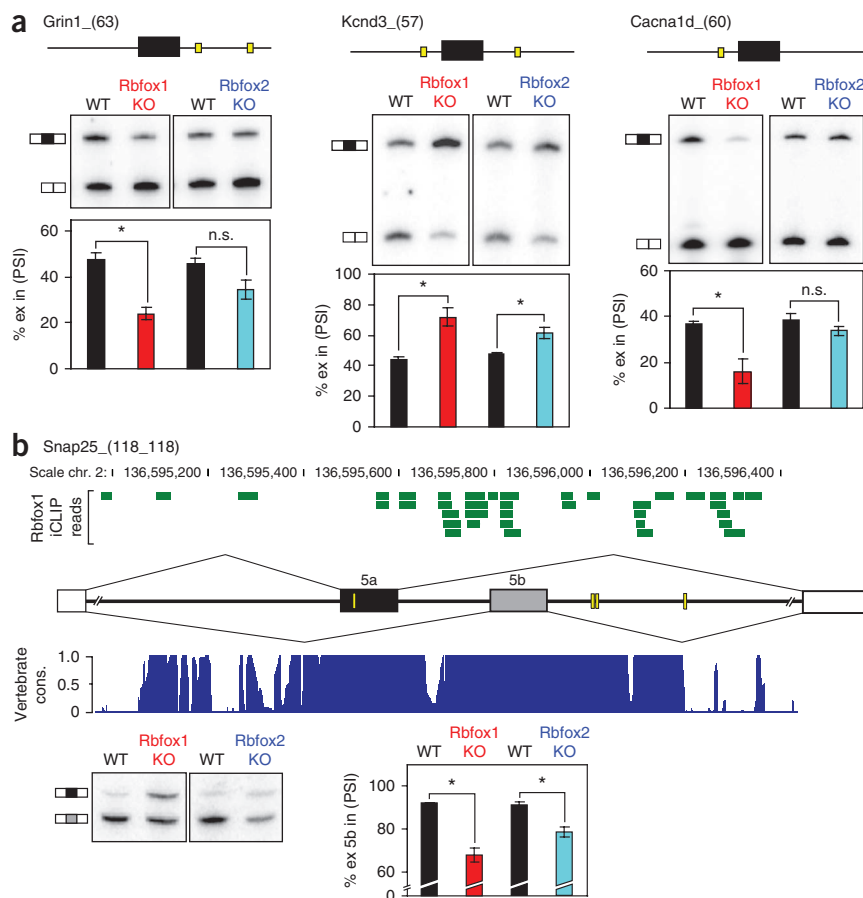
Nearly all of the identified exons possess (U)GCAUG motifs in their flanking introns and are likely to be directly regulated by *Rbfox1*. In total, 85% of exons (11 out of 13) showing reduced inclusion in the *Rbfox1^{-/-}* brain contain a (U)GCAUG within the proximal 300 nucleotides downstream of the exon, consistent with a loss of *Rbfox1* activation; 86% of exons (6 out of 7) showing increased inclusion have a *Rbfox1* binding site within 300 nucleotides upstream, consistent with

Table 1 Summary of differentially spliced exons in *Rbfox1^{-/-}* brain

	Alt event ID ^a	Δ PSI (mean \pm s.e.m.) ^b	P^c	Upstream (U)GCAUG ^d	Downstream (U)GCAUG ^d	Function ^e
1	Stx3_(46)	-33.44 \pm 3.65	0.00587	(-101, -74)	(+25, +185, +195)	SNARE complex
2	Snap25_(118_118)	-24.24 \pm 3.27	0.00886	n/p_n/p	n/p_(+94, +101, +287)	SNARE complex
3	Grin1_(63)	-23.29 \pm 2.66	0.00641	n/p	(+8, +262)	Neurotransmitter receptor
4	Camta1_(31)	-22.16 \pm 1.94	0.00378	n/p	(+70, +210, +252)	Calmodulin binding
5	Cacna1s_(57)	-21.46 \pm 2.61	0.00724	n/p	(+13, +44, +60, +69, +165)	Ion channel
6	Cacna1d_(60)	-20.64 \pm 5.03	0.02726	(-47)	n/p	Ion channel
7	Gabrg2_(24)	-13.73 \pm 2.14	0.01173	n/p	(+30)	Neurotransmitter receptor
8	Scn8a_(92_92)	-12.33 \pm 0.81	0.00216	n/p_n/p	n/p_(+114, +192)	Ion channel
9	Camk2g_(68)	-11.30 \pm 1.13	0.00496	(-264, -65)	(+8, +65, +120, +190)	Calmodulin binding
10	Nrxn3_(27)	-7.61 \pm 1.30	0.01400	n/p	n/p	Synapse assembly
11	Ablim1_(120)	-6.93 \pm 0.93	0.00871	(-255)	(+123, +171)	Cytoskeletal dynamics
12	Cadps_(147)	-6.11 \pm 1.49	0.02745	(-227)	(+49)	SNARE complex
13	Tpm3_(79)	+1.92 \pm 0.31	0.01277	(-260)	n/p	Cytoskeletal dynamics
14	Nrcam_(57)	+5.46 \pm 0.69	0.00773	(-136)	(+171)	Synapse assembly
15	Ptpro_(84)	+6.97 \pm 2.22	0.04400	n/p	n/p	Tyr phosphatase
16	Cacna1d_(104_104)	+7.63 \pm 2.35	0.04180	(-225, -191)_n/p	n/p_(+93)	Ion channel
17	Ppp3ca_(30)	+8.55 \pm 1.97	0.02465	(-188)	n/p	Calmodulin binding
18	Pbrm1_(156)	+13.22 \pm 2.52	0.01729	(-78, -44, -31)	(+233)	Chromatin binding
19	Stxbp5l_(72)	+13.57 \pm 4.51	0.04757	(-13)	(+130)	SNARE complex
20	Kcnd3_(57)	+28.17 \pm 7.63	0.03233	(-16)	(+83)	Ion channel

^aThe number in parenthesis after the gene ID indicates the size in nucleotides of the alternative exon. All events listed are alternative cassette exons, except those with two exon sizes (for example, Snap25_(118_118)), which are paired mutually exclusive exons. ^b Δ PSI, percent change in alternative exon inclusion for *Rbfox1^{-/-}* brain compared to wild type, determined by RT-PCR. For mutually exclusive exons, the value given is for the downstream exon. ^cThe RT-PCR P value was determined by paired, one-tailed Student's t test ($n = 3$). ^dLocation of (U)GCAUG binding sites in the proximal 300 nucleotides upstream and downstream of the alternative exon are shown with distance in nucleotides in parenthesis. ^eReported function of the encoded protein, as determined from literature citations. n/p, not present.

Figure 3 *Rbfox1*^{-/-} brain exhibits splicing changes in transcripts affecting synaptic function and neuronal excitation. **(a)** Denaturing gel electrophoresis of RT-PCR products for three *Rbfox1*-dependent exons. Above each gel is a schematic depicting the alternative exon (horizontal black box) and the relative location of (U)GCAUG binding sites (yellow boxes) in the flanking introns (thin horizontal lines). Shown below each gel is a graph quantifying the mean percentage of alternative exon inclusion (% ex in, PSI) in wild-type (black bars), *Rbfox1* knockout (KO; red bars) and *Rbfox2* knockout (blue bars) brain. **(b)** A schematic showing the *Snap25* mutually exclusive exon pair, 5a (horizontal black box) and 5b (horizontal gray box), plus the intervening intron and the proximal 500 nucleotides of the adjacent introns. Yellow boxes represent (U)GCAUG motifs. The distribution of *Rbfox1* iCLIP reads (horizontal green bars) is shown above. A histogram displaying the conservation of this region among 30 vertebrate species as determined by phastCons (see URLs) is shown below. A score of 1 indicates 100% identity among all species at that nucleotide position. Chromosomal location in nucleotides is shown above the iCLIP data. At the bottom, the RT-PCR assay and quantification of exons 5a and 5b splicing is shown, with the inclusion of the downstream exon plotted. For **a** and **b**, error bars represent s.e.m.; *n* = 3. **P* < 0.05 and n.s. means not significant by paired, one-tailed Student's *t* test. Exact *P* values are shown in **Table 1**.



a loss of *Rbfox1* repression (**Table 1**). This represents a substantial enrichment of *Rbfox1* binding motifs in the knockout-responsive exons. Of the 5,166 alternative cassette exons probed by the MJAY array, only 1,590 (31%) have a (U)GCAUG motif within 300 nucleotides downstream and only 1,328 (26%) have this motif within 300 nucleotides upstream. Characterization of *Rbfox1* binding sites in mouse cortex using individual-nucleotide resolution crosslinking immunoprecipitation (iCLIP)^{12,34} confirms that a majority of these exons show adjacent *Rbfox1* binding *in vivo* and are thus direct targets of the protein (**Fig. 3b** and data not shown). Notably, there were minimal changes in the overall expression of genes across the array. Besides the expected loss of *Rbfox1* mRNA, we detected only two changes in transcript abundance in the *Rbfox1*^{-/-} brain (Pop4 and AK138161, encoding a hypothetical protein expressed in mouse hypothalamus). The effect of *Rbfox1* is primarily post-transcriptional. We also examined the protein expression of several well-characterized splicing

factors in the *Rbfox1*^{-/-} brain. Most of the proteins tested, including *Ptbp1* (PTB) and *Mbnl1*, were unchanged in the *Rbfox1*^{-/-} brain. The neuron-specific splicing factor *Nova1* was moderately decreased (**Supplementary Fig. 4**). *Rbfox1* apparently affects the post-transcriptional regulation of *Nova1*, with loss of *Rbfox1* resulting in reduced *Nova1* expression. This is notable in light of previous findings of a substantial overlap between the *Nova1* and *Rbfox1* protein regulatory networks³⁵. It is also notable that *Rbfox1* targets are enriched in synaptic functions, similar to *Nova1*.

The splicing changes in the *Rbfox1*^{-/-} brain affect multiple functional components of synaptic transmission that could clearly contribute to the epileptic phenotype (**Table 1**). Transcripts for ion channels such as the voltage-gated potassium channel *K_v4.3* (encoded by *Kcnd3*) and the L-type calcium channel subunits *Ca_v1.1 α* (encoded by *Cacna1s*) and *Ca_v1.3 α 1* (encoded by *Cacna1d*) were significantly altered in the *Rbfox1*^{-/-} brain (see **Table 1** for

Table 2 Summary of transcripts altered in *Rbfox1*^{-/-} brain with implications in epilepsy

Gene	Protein	Implications in epilepsy	Splicing change in <i>Rbfox1</i> KO brain	Effect of splicing change on encoded protein	
1	Gabrg2	GABA-A receptor γ 2	Mutations identified in affected individuals ³⁷	Decrease in exon 9 inclusion	Removes a protein kinase C phosphorylation site that modulates receptor function
2	Grin1	NMDA receptor 1	Downregulation reduces seizure susceptibility in mice ^{38,39}	Decrease in exon 5 inclusion	Removes a portion of the extracellular domain, altering the receptor's response to ligands
3	Scn8a	Na(v)1.6 sodium channel	Mouse mutations exhibit seizures ⁴⁰	Decrease in exon 5A	Modifies transmembrane segments S3 and S4 of domain I; results in decreased expression of the adult isoform
4	Snap25	SNAP-25	Mouse mutations exhibit seizures ⁴¹	Decrease in exon 5b	Modifies the N terminus; results in decreased expression of the adult isoform

KO, knockout.

P values). Transcripts encoding neurotransmitter receptors such as the gamma-aminobutyric acid (GABA)-A receptor subunit $\gamma 2$ (encoded by *Gabrg2*) and the NMDA receptor 1 (encoded by *Grin1*) were also changed in the *Rbfox1*^{-/-} brain. We also found splicing changes in transcripts for structural proteins of the synapse, such as neuexin 3 (encoded by *Nrxn3*) and for vesicle fusion proteins including syntaxin 3 (encoded by *Stx3*), synaptosomal-associated protein 25 (encoded by *Snap25*) and the calcium-dependent secretion activator (encoded by *Cadps*). Changes in intracellular calcium dynamics are associated with epileptogenesis, including alterations in calcium entry through voltage-gated channels or changes in calcium buffering by calcium-binding proteins³⁶. In addition to the splicing changes in the voltage-gated channels mentioned above, we identified changes in transcripts for the calcium/calmodulin-dependent protein kinase II (encoded by *Camk2g*), the calmodulin binding transcription activator (encoded by *Camta1*) and the calmodulin-dependent calcineurin subunit (encoded by *Ppp3ca*). Disruption of calcium dynamics may contribute to the epileptic phenotype observed in *Rbfox1*^{loxP/loxP}; *Nestin-Cre*^{+/-} mice.

Most notably, a number of the *Rbfox1* target transcripts have been directly linked to epilepsy (Table 2). Mutations in *Gabrg2* have been identified in humans with epilepsy³⁷, and changes in expression of NMDA receptor 1 (encoded by *Grin1*) or the voltage-gated sodium channel Na_v1.6 (encoded by *Scn8a*) alter seizure susceptibility in mice^{38–40}. Transgenic mouse models have revealed that changes in expression or alternative splicing of *Snap25* result in seizures^{41,42}. In particular, it was found that the splicing ratio of a pair of *Snap25* mutually exclusive exons is developmentally regulated and that removal of the exon 5b predominantly expressed in adult brain results in spontaneous seizures⁴². We find that the splicing of this same adult-specific exon is reduced by 24% in the *Rbfox1*^{-/-} brain and is reduced by a much lesser extent (12%) in the *Rbfox2*^{-/-} brain (Table 1 and Fig. 3b). We also identified a number of *Rbfox1* iCLIP reads surrounding (U)GCAUG motifs adjacent to exon 5b (Fig. 3b), indicating that *Rbfox1* directly regulates the splicing of this exon. The change in *Rbfox1*-dependent *Snap25* splicing likely contributes to the seizure phenotype of *Rbfox1* knockout mice.

In summary, our findings show a critical role for *Rbfox1* in neuronal function. We previously showed that changes in *Rbfox1* activity in response to chronic stimuli can homeostatically adjust the level of splicing for its target exons²⁴. The limited response of *Rbfox2* and *Rbfox3* to depolarizing media (Ji-Ann Lee & D.L.B., unpublished observations) and the abnormal physiology of the *Rbfox1* knockout brain indicate that these proteins are not fully redundant in their functions and that *Rbfox1* plays a unique role in the cellular response to overexcitation. The *Rbfox1* knockout mice provide a new model for examining how modifications of synaptic proteins determine excitation and epileptogenesis. Splicing regulation by *Rbfox1* clearly affects neuronal excitation. However, the presence of cytoplasmic *Rbfox1* protein and its binding to 3' untranslated regions indicates that there will be other components to the *Rbfox1*^{-/-} phenotype. Examination of the larger nuclear and cytoplasmic programs of post-transcriptional regulation by *Rbfox1* should yield new insights into the control of cellular homeostasis and its misregulation in neurological disease.

URLs. phastCons, <http://genome.ucsc.edu/>.

METHODS

Methods and any associated references are available in the online version of the paper at <http://www.nature.com/naturegenetics/>.

Accession codes. The full dataset is available online at Gene Expression Omnibus (GEO) at <http://www.ncbi.nlm.nih.gov/geo/query/acc.cgi?acc=GSE28421>.

Note: Supplementary information is available on the Nature Genetics website.

ACKNOWLEDGMENTS

This work was done in collaboration with X.-D. Fu (University of California, San Diego). We thank N. Copeland (Institute of Molecular and Cell Biology, Singapore) for the recombinering vectors and bacterial strains used for generating the transgenic *Rbfox1* mice and J.P. Donahue for his help with the microarray analyses. D. Geschwind, K. Martin and T. Nilsen gave us helpful comments on the manuscript. This work was supported in part by US National Institutes of Health Grants R01 GM049369 to X.D.F., R37 NS30549 and R01 MH076994 to I.M., R01 GM084317 to M.A. and D.L.B., and R01 GM49662 to D.L.B. D.L.B. is an Investigator of the Howard Hughes Medical Institute.

AUTHOR CONTRIBUTIONS

Project conception: D.L.B., P.S. and L.T.G. **Creation of transgenic mice:** P.S. **Phenotypic analysis, histology, immunofluorescence and RT-PCR studies:** L.T.G. **Behavioral seizure analyses:** J.M., L.T.G. and I.M. **Electrophysiology:** J.M. and I.M. **iCLIP study:** A.D. and C.-H.L. **Microarray studies:** L.S., L.T.G. and M.A. **Manuscript preparation:** L.T.G. and D.L.B.

COMPETING FINANCIAL INTERESTS

The authors declare no competing financial interests.

Published online at <http://www.nature.com/naturegenetics/>.

Reprints and permissions information is available online at <http://www.nature.com/reprints/index.html>.

- Kuroyanagi, H. Fox-1 family of RNA-binding proteins. *Cell. Mol. Life Sci.* **66**, 3895–3907 (2009).
- Li, Q., Lee, J.A. & Black, D.L. Neuronal regulation of alternative pre-mRNA splicing. *Nat. Rev. Neurosci.* **8**, 819–831 (2007).
- Licatalosi, D.D. & Darnell, R.B. Splicing regulation in neurologic disease. *Neuron* **52**, 93–101 (2006).
- Jin, Y. *et al.* A vertebrate RNA-binding protein Fox-1 regulates tissue-specific splicing via the pentanucleotide GCAUG. *EMBO J.* **22**, 905–912 (2003).
- Nakahata, S. & Kawamoto, S. Tissue-dependent isoforms of mammalian Fox-1 homologs are associated with tissue-specific splicing activities. *Nucleic Acids Res.* **33**, 2078–2089 (2005).
- Underwood, J.G., Boutz, P.L., Dougherty, J.D., Stoilov, P. & Black, D.L. Homologues of the *Caenorhabditis elegans* Fox-1 protein are neuronal splicing regulators in mammals. *Mol. Cell. Biol.* **25**, 10005–10016 (2005).
- Auweter, S.D. *et al.* Molecular basis of RNA recognition by the human alternative splicing factor Fox-1. *EMBO J.* **25**, 163–173 (2006).
- Black, D.L. Activation of c-src neuron-specific splicing by an unusual RNA element *in vivo* and *in vitro*. *Cell* **69**, 795–807 (1992).
- Huh, G.S. & Hynes, R.O. Regulation of alternative pre-mRNA splicing by a novel repeated hexanucleotide element. *Genes Dev.* **8**, 1561–1574 (1994).
- Zhang, C. *et al.* Defining the regulatory network of the tissue-specific splicing factors Fox-1 and Fox-2. *Genes Dev.* **22**, 2550–2563 (2008).
- Yeo, G.W. *et al.* An RNA code for the FOX2 splicing regulator revealed by mapping RNA-protein interactions in stem cells. *Nat. Struct. Mol. Biol.* **16**, 130–137 (2009).
- Shibata, H., Huynh, D.P. & Pulst, S.M. A novel protein with RNA-binding motifs interacts with ataxin-2. *Hum. Mol. Genet.* **9**, 1303–1313 (2000).
- Bhalla, K. *et al.* The *de novo* chromosome 16 translocations of two patients with abnormal phenotypes (mental retardation and epilepsy) disrupt the A2BP1 gene. *J. Hum. Genet.* **49**, 308–311 (2004).
- Barnby, G. *et al.* Candidate-gene screening and association analysis at the autism-susceptibility locus on chromosome 16p: evidence of association at *GRIN2A* and *ABAT*. *Am. J. Hum. Genet.* **76**, 950–966 (2005).
- Martin, C.L. *et al.* Cytogenetic and molecular characterization of *A2BP1/FOX1* as a candidate gene for autism. *Am. J. Med. Genet. B. Neuropsychiatr. Genet.* **144B**, 869–876 (2007).
- Sebat, J. *et al.* Strong association of *de novo* copy number mutations with autism. *Science* **316**, 445–449 (2007).
- Kiehl, T.R., Shibata, H., Vo, T., Huynh, D.P. & Pulst, S.M. Identification and expression of a mouse ortholog of *A2BP1*. *Mamm. Genome* **12**, 595–601 (2001).
- Ponthier, J.L. *et al.* Fox-2 splicing factor binds to a conserved intron motif to promote inclusion of protein 4.1R alternative exon 16. *J. Biol. Chem.* **281**, 12468–12474 (2006).
- Yeo, G.W. *et al.* Alternative splicing events identified in human embryonic stem cells and neural progenitors. *PLoS Comput. Biol.* **3**, 1951–1967 (2007).

21. McKee, A.E. *et al.* A genome-wide in situ hybridization map of RNA-binding proteins reveals anatomically restricted expression in the developing mouse brain. *BMC Dev. Biol.* **5**, 14 (2005).
22. Kim, K.K., Adelstein, R.S. & Kawamoto, S. Identification of neuronal nuclei (NeuN) as Fox-3, a new member of the Fox-1 gene family of splicing factors. *J. Biol. Chem.* **284**, 31052–31061 (2009).
23. Kim, K.K., Kim, Y.C., Adelstein, R.S. & Kawamoto, S. Fox-3 and PSF interact to activate neural cell-specific alternative splicing. *Nucleic Acids Res.* (2011).
24. Lee, J.A., Tang, Z.Z. & Black, D.L. An inducible change in Fox-1/A2BP1 splicing modulates the alternative splicing of downstream neuronal target exons. *Genes Dev.* **23**, 2284–2293 (2009).
25. Damianov, A. & Black, D.L. Autoregulation of Fox protein expression to produce dominant negative splicing factors. *RNA* **16**, 405–416 (2010).
26. Tang, Z.Z., Zheng, S., Nikolic, J. & Black, D.L. Developmental control of CaV1.2 L-type calcium channel splicing by Fox proteins. *Mol. Cell. Biol.* **29**, 4757–4765 (2009).
27. Tronche, F. *et al.* Disruption of the glucocorticoid receptor gene in the nervous system results in reduced anxiety. *Nat. Genet.* **23**, 99–103 (1999).
28. Graus-Porta, D. *et al.* Beta1-class integrins regulate the development of laminae and folia in the cerebral and cerebellar cortex. *Neuron* **31**, 367–379 (2001).
29. Herrera, D.G. & Robertson, H.A. Activation of c-fos in the brain. *Prog. Neurobiol.* **50**, 83–107 (1996).
30. Bertram, E.H. Temporal lobe epilepsy: where do the seizures really begin? *Epilepsy Behav.* **14** (Suppl 1), 32–37 (2009).
31. Ben-Ari, Y. Limbic seizure and brain damage produced by kainic acid: mechanisms and relevance to human temporal lobe epilepsy. *Neuroscience* **14**, 375–403 (1985).
32. Racine, R.J. Modification of seizure activity by electrical stimulation. II. Motor seizure. *Electroencephalogr. Clin. Neurophysiol.* **32**, 281–294 (1972).
33. Ule, J. *et al.* Nova regulates brain-specific splicing to shape the synapse. *Nat. Genet.* **37**, 844–852 (2005).
34. König, J. *et al.* iCLIP reveals the function of hnRNP particles in splicing at individual nucleotide resolution. *Nat. Struct. Mol. Biol.* **17**, 909–915 (2010).
35. Zhang, C. *et al.* Integrative modeling defines the Nova splicing-regulatory network and its combinatorial controls. *Science* **329**, 439–443 (2010).
36. Delorenzo, R.J., Sun, D.A. & Deshpande, L.S. Cellular mechanisms underlying acquired epilepsy: the calcium hypothesis of the induction and maintenance of epilepsy. *Pharmacol. Ther.* **105**, 229–266 (2005).
37. Mulley, J.C., Scheffer, I.E., Petrou, S. & Berkovic, S.F. Channelopathies as a genetic cause of epilepsy. *Curr. Opin. Neurol.* **16**, 171–176 (2003).
38. Chapman, A.G., Woodburn, V.L., Woodruff, G.N. & Meldrum, B.S. Anticonvulsant effect of reduced NMDA receptor expression in audiogenic DBA/2 mice. *Epilepsy Res.* **26**, 25–35 (1996).
39. Zapata, A. *et al.* Effects of NMDA-R1 antisense oligodeoxynucleotide administration: behavioral and radioligand binding studies. *Brain Res.* **745**, 114–120 (1997).
40. Papale, L.A. *et al.* Heterozygous mutations of the voltage-gated sodium channel SCN8A are associated with spike-wave discharges and absence epilepsy in mice. *Hum. Mol. Genet.* **18**, 1633–1641 (2009).
41. Corradini, I., Verderio, C., Sala, M., Wilson, M.C. & Matteoli, M. SNAP-25 in neuropsychiatric disorders. *Ann. NY Acad. Sci.* **1152**, 93–99 (2009).
42. Johansson, J.U. *et al.* An ancient duplication of exon 5 in the *Snap25* gene is required for complex neuronal development/function. *PLoS Genet.* **4**, e1000278 (2008).

ONLINE METHODS

Mice. We used homologous recombination to create 'floxed' *Rbfox1* alleles consisting of *loxP* sites flanking *Rbfox1* exons 11 and 12, annotated as previously described²⁵. DNA blot hybridization probes were generated by PCR amplification (Supplementary Table 3), cloned using the TOPO TA cloning kit (Invitrogen) and labeled by PCR in the presence of α -³²P-dCTP. Mouse strain 129S6/SVEvTac BAC library (RPC1-22), arrayed on high density nylon filters, was obtained from Children's Hospital Oakland Research Institute (CHORI), and probe *Rbfox1_knpr_frt* was used to screen the BAC library. Positive clones were purchased from CHORI and validated by BAC end sequencing. Clone RP22-344J23 was used to construct the floxed *Rbfox1* targeting cassette also carrying a neomycin resistance (*neo*) cassette flanked by *Frt* sites⁴³, and the primer sequences used for recombineering are listed in Supplementary Table 3. The targeting cassette was transfected into 129S2/Sv embryonic stem cells at the University of California, San Diego (UCSD) Transgenic and Gene Targeting Core. Clones that had undergone homologous recombination were identified by DNA blot using the 5' and 3' probes after digesting the genomic DNA with *Swa*I and *Spe*I (Supplementary Fig. 1). Cells from positive clones were injected into a C57BL/6J blastocyst at the UCSD transgenic and gene targeting core, and one line was found to have germline transmission. Heterozygous (*Rbfox1*^{loxP/+}) F1 offspring were crossed to transgenic mice expressing Flp recombinase⁴⁴ to excise the *neo* cassette. Resulting heterozygous (*Rbfox1*^{loxP/+}) mice lacking the *neo* cassette were intercrossed to produce homozygous (*Rbfox1*^{loxP/loxP}) mice. Homozygous mice were then crossed to transgenic *Nestin-Cre*^{+/-} mice, allowing for restricted deletion of *Rbfox1* in the CNS of double transgenic mice (*Rbfox1*^{loxP/loxP}; *Nestin-Cre*^{+/-}). Primers used for genotyping the *Rbfox1*⁺, *Rbfox1*^{loxP} and *Rbfox1*^Δ alleles are listed in Supplementary Table 3, and product sizes are given in Supplementary Figure 1. Mice used for this study were maintained on a mixed 129S2/Sv × C57BL/6J background. Animals were housed in a 12-h light-dark cycle with food and water available *ad libitum* and were maintained by the University of California, Los Angeles (UCLA) Association for Assessment and Accreditation of Laboratory Animal Care accredited Division of Laboratory Medicine. All experiments were Institutional Animal Care and Use Committee approved by the UCLA Chancellor's Animal Research Council.

Protein blotting. Nuclei were isolated from wild-type, *Rbfox1*^{+/-} and *Rbfox1*^{-/-} brains as previously described⁴⁵. Nuclei were lysed in Lysis Buffer (20 mM Hepes-KOH, pH 7.9, 300 mM NaCl, 1 mM EDTA, 0.75% NP-40) containing complete protease inhibitors (Roche) for 10 min on ice. For quantification of synaptic proteins or splicing factors, hippocampi or total brains, respectively, were dissected from wild-type and *Rbfox1*^{loxP/loxP}; *Nestin-Cre*^{+/-} mice and homogenized by sonication in RIPA buffer containing protease inhibitors. Nuclear and total protein samples were cleared, boiled in SDS loading buffer and resolved on 10% Tris-glycine gels. Antibodies were used at the following dilutions: α -Rbfox1 1D10²⁴, 1:2,000; α -Rbfox2, 1:2,000 (Bethyl); α -U1-70K, 1:5,000; α -Synapsin-I, 1:2,000 (Millipore); α -PSD-95, 1:2,000 (Millipore); α -GAPDH, 1:10,000 (Ambion); α -PTB NT4856, 1:2,500; α -nPTB IS2, 1:3,000; α -Mbn1, 1:1,000 (Millipore); α -Nova-1, 1:1,000 (Millipore); α -hnRNPA1, 1:1,000; α -SRp20, 1:1,500 (Zymed); α - β -tubulin, 1:100 (Santa Cruz); and ECL Plex Cy3-conjugated goat α -mouse and Cy5-conjugated goat α -rabbit secondary antibodies, 1:2,500 (GE Healthcare).

Histology and immunohistochemistry. *Rbfox1*^{loxP/loxP}; *Nestin-Cre*^{+/-} and wild-type littermates were transcardially perfused with ice-cold 0.1 M phosphate buffered saline (PBS; pH 7.4) followed by ice-cold 4% paraformaldehyde in PBS (pH 7.4). Brains were cryoprotected in 30% sucrose, and 40 μ m free-floating sections were cut in the coronal orientation using a Microm HM505E cryostat. For Nissl histology, sections were hydrated and stained using 0.25% thionin acetate (Sigma), dehydrated through alcohols, cleared in xylenes and mounted with DPX (Electron Microscopy Sciences). For double immunofluorescent staining, sections were blocked for 30 min with blocking solution (10% normal goat serum, 0.1% Triton X-100 in PBS) and incubated with primary antibodies at 4 °C overnight. Sections were washed three times and stained with secondary antibodies in PBS for 2 h. Sections were again washed three times, mounted with ProLong Gold plus DAPI reagent (Invitrogen) and imaged using a Zeiss LSM 510 Meta confocal microscope. The following

primary antibodies were used: α -Rbfox1 1D10, 1:200; α -Rbfox2, 1:200 (Bethyl); and α -c-Fos Ab-5, 1:1,600 (Calbiochem). Alexa Fluor 488-conjugated goat α -mouse IgG and Alexa Fluor 568-conjugated goat α -rabbit IgG secondary antibodies (Molecular Probes) were used at a dilution of 1:1,000. For Golgi-Cox staining, wild-type and *Rbfox1*^{-/-} brains were processed using the FD Rapid GolgiStain Kit (FD Neurotechnologies) according to the manufacturer's instructions and counterstained with thionin acetate. For spine quantification, the analyzer was blind to the experimental group throughout the analysis. Dendrites of the same size in diameter from dentate gyrus granule cells were randomly selected from four slices per individual animal. A total of 28–29 dendritic segments from two animals per genotype were used for quantification. Images were collected under a 100 \times oil-immersion objective using the Spot RT KE camera and software system (Diagnostic Instruments). Spines were operationally defined as any protrusion less than 5 μ m in length. Each spine was manually traced, and dendritic length was measured using ImageJ software. The spine numbers were expressed as mean spine density per 10 μ m of linear dendritic length. For all histology and immunofluorescence experiments, images shown are representative of at least two independent samples.

Behavioral observation of kainic acid-induced seizures. Kainic acid (Sigma) was dissolved in sterile saline and administered intraperitoneally at 20 mg/kg body weight. Ten wild-type mice, four heterozygous *Rbfox1*^{loxP/+}; *Nestin-Cre*^{+/-} mice, four homozygous *Rbfox1*^{loxP/loxP}; *Nestin-Cre*^{+/-} mice and four homozygous *Rbfox2*^{loxP/loxP}; *Nestin-Cre*^{+/-} mice (2–3 months of age) were used. In all experiments, the experimenter was blind to the genotype of the animals, and each experiment used at least one wild-type littermate. Seizure severity was determined according to the Racine Scale³²: stage 0, normal behavior; stage 1, mouth and facial movements; stage 2, head bobbing; stage 3, forelimb clonus; stage 4, rearing; stage 5, continuous rearing and falling (tonic-clonic seizures); and stage 6, status epilepticus and/or death. For each animal, the seizure score was determined every 10 min for 2 h after kainic acid administration. Each animal's maximum score for each 10 min interval was used to calculate the mean seizure score (\pm s.e.m.) for each experimental group. Latency to the first stage 5 (tonic-clonic) seizure, duration of each stage 5 seizure and time to death were measured from time of kainic acid administration. Statistical significance was determined using a one-tailed Student's *t* test. The level of significance was set as $P < 0.05$.

Electrophysiology. To obtain synaptic I/O curves, hippocampal field potential recordings were carried out as previously described⁴⁶. Coronal hippocampal slices (350 μ m thick) were prepared from three adult (2–3 months old) wild-type and three *Rbfox1*^{loxP/loxP}; *Nestin-Cre*^{+/-} mice. Hippocampal field recordings were performed at 32–34 °C under standard conditions in an interface chamber perfused with normal artificial cerebral spinal fluid (nACSF) solution containing (in mM): 126 NaCl, 2.5 KCl, 2 CaCl₂, 1–2 MgCl₂, 1.25 NaHPO₄, 26 NaHCO₃ and 10 D-glucose, pH 7.3–7.4 (bubbled with 95% O₂ and 5% CO₂). Field potentials were evoked by lateral perforant path stimulation at 0.05 Hz, and responses were recorded in the dentate gyrus molecular layer. Bipolar electrodes were used to deliver a constant-current stimulus. The stimulus intensity was determined by recording a threshold response at a width (*W*) of 60 μ s with no response at 20 μ s. The *W* of the stimulus was increased stepwise by 20 μ s to create I/O curves ranging from 20 to 240 μ s. Four population field EPSPs (fEPSPs) were recorded at each *W*, and the maximum slope of the responses (volts per second) was measured over a 0.5–1 ms window of the fEPSP rising phase. The average slope was calculated at each *W* used. I/O curves were fit with a Boltzmann equation: $f(W) = (\text{MAX}/(1 + \exp((W - W_{50})/k))) + \text{MAX}$, where *W* is stimulus width, MAX is the maximum response, *k* is a slope factor and *W*₅₀ is the stimulus width that elicits 50% of MAX. The fitted parameters were compared between experimental groups, and statistical significance was determined using a one-way ANOVA followed by Bonferroni's corrected *t*-tests.

Splicing microarrays. Total RNA was extracted by Trizol reagent (Invitrogen) from whole brain of three wild-type and three *Rbfox1*^{loxP/loxP}; *Nestin-Cre*^{+/-} mice, all of which were 1-month-old males. Ribosomal RNAs were removed from samples using the RiboMinus Transcriptome Isolation Kit (Invitrogen) according to the manufacturer's instructions. An amplified, biotinylated

complementary DNA target was produced using the GeneChip Whole Transcript Sense Target Labeling and Control Reagents kit (Affymetrix) according to the manufacturer's instructions. Each sample target was hybridized overnight to a Mouse GeneSplice Array (Affymetrix PN 540092). Hybridized arrays were processed using the Affymetrix Fluidics Station 450 and scanned with an Affymetrix GeneChip scanner. Data were analyzed, and each alternative event was assigned an MJAY ratio, a measure of the difference in the average ratio of inclusion to skipping the indicated exon in the *Rbfox1*^{-/-} samples compared to wild-type, as previously described⁴⁷. The top 25 significant changes, ranked in descending order by the absolute value of the MJAY ratio, of alternative cassettes and mutually exclusive exons are shown in **Supplementary Table 2**.

RT-PCR assay. Total RNA was extracted by Trizol reagent (Invitrogen) from whole brain of 1-month-old wild-type, *Rbfox1*^{loxP/loxP}; *Nestin-Cre*^{+/-} and *Rbfox2*^{loxP/loxP}; *Nestin-Cre*^{+/-} mice ($n = 3$ for each genotype). We reverse transcribed 1 μ g of total RNA with random hexamers. One-tenth of this reaction was then amplified in 24 cycles of PCR with exon-specific primers, one of which was ³²P-labeled. The PCR products were resolved on 8% polyacrylamide, 7.5 M urea denaturing gels. The gel was dried, exposed and scanned in a Typhoon 9400 PhosphorImager scanner (GE Healthcare). Images were analyzed with ImageQuant TL Software. The mean exon inclusion levels were calculated for wild-type and *Rbfox1*^{-/-} brains, and the percent change in inclusion (Δ PSI) was calculated by subtracting the *Rbfox1*^{-/-} mean inclusion level from the wild-type mean inclusion level. Statistical significance was determined using the paired, one-tailed Student's *t* test with significance set to $P < 0.05$. RT-PCR primers are listed in **Supplementary Table 3**.

Rbfox1-RNA crosslinking immunoprecipitation analysis (Rbfox1 iCLIP). The Rbfox1 iCLIP was done as previously described³⁴ with the following modifications: cortices from 1.5-month-old male and female wild-type

C57BL/6J mice were dissected, triturated in 8 ml ice cold HBSS with 20 mM HEPES-KOH pH 7.5, and ultraviolet irradiated in a Stratilinker 1800 (Stratagene) at 750 mJ/cm². Rbfox1 was immunoprecipitated with 1D10 antibody and washed with high salt buffer. The immobilized crosslinked RNA was fragmented as previously described¹²: aliquots of beads in 50 μ l of 1 \times micrococcal nuclease buffer with 5.0 μ g yeast transfer RNA were treated with 5 or 2,000 Kunz U/ml of micrococcal nuclease (New England Biolabs) for 5 min at 37 °C. The enzyme was inhibited by addition of 0.5 ml 1 \times PNK buffer + EGTA. The RNA fragments were dephosphorylated for 1 h to remove the 3' phosphorylates left by micrococcal nuclease. The RNA linker contained 3' biotin instead of the puromycin group used previously³⁴. Because Rbfox1 co-migrates with the IgG heavy chain, the crosslinked protein-RNA-linker products were purified on monomeric avidin beads (Fischer Scientific) before resolving on 10% NuPAGE gel (Invitrogen). The constructed Rbfox1 iCLIP library was sequenced on a Genome Analyzer Iix (Illumina) with a 76 nucleotide read length. Mapping of sequence reads was performed against the mouse genome (version mm9/NCBI37) using Bowtie version 0.12.5 (ref. 48) as previously described³⁴.

43. Liu, P., Jenkins, N.A. & Copeland, N.G. A highly efficient recombineering-based method for generating conditional knockout mutations. *Genome Res.* **13**, 476–484 (2003).
44. Farley, F.W., Soriano, P., Steffen, L.S. & Dymecki, S.M. Widespread recombinase expression using FLP_{eR} (flipper) mice. *Genesis* **28**, 106–110 (2000).
45. Grabowski, P.J. Splicing-active nuclear extracts from rat brain. *Methods* **37**, 323–330 (2005).
46. Maguire, J., Ferando, I., Simonsen, C. & Mody, I. Excitability changes related to GABAA receptor plasticity during pregnancy. *J. Neurosci.* **29**, 9592–9601 (2009).
47. Sugnet, C.W. *et al.* Unusual intron conservation near tissue-regulated exons found by splicing microarrays. *PLOS Comput. Biol.* **2**, e4 (2006).
48. Langmead, B., Trapnell, C., Pop, M. & Salzberg, S.L. Ultrafast and memory-efficient alignment of short DNA sequences to the human genome. *Genome Biol.* **10**, R25 (2009).